Simulation of Electrical Rotor Asymmetries in Squirrel Cage Induction Machines with the ExtendedMachines Library

Christian Kral Anton Haumer
Arsenal Research
Giefinggasse 2, 1210 Vienna, Austria
christian.kral@arsenal.ac.at

Abstract

In this paper a physical model of a squirrel cage induction machine with rotor topology model is presented. The parameters of the induction machine are discussed and the issue of rotor fault detection is addressed. For a machine with one broken rotor bar a Modelica simulation model is compared with measurement results.
Keywords: Electric machines, squirrel cage, rotor asymmetries

1 Introduction

The squirrel cage of an induction machine consists of N_r bars and two end rings, connecting the bars on both ends, as depicted in Fig. 1. The fins located on the end rings are required to force the circulation of the air in the inner region of the machine.
In the manufacturing process it is intended to fabricate a fully symmetrical squirrel cage. Due to manufacturing problems or certain operating conditions, electrical rotor asymmetries can occur. The causes for such rotor electrical asymmetries are:

- shrink holes and voids in the aluminum of the bars or end rings,
- improper junctions of the bars and end rings,
- heavy duty start-ups that the machine is not designed for,
- thermal overloading of the machine,
- high temperature gradients, causing cracks.

Electric rotor asymmetry can be classified as rotor bar or a rotor end ring segment fault. These cases can be modeled by a ohmic resistance increase of either a rotor bar or an end ring segment.

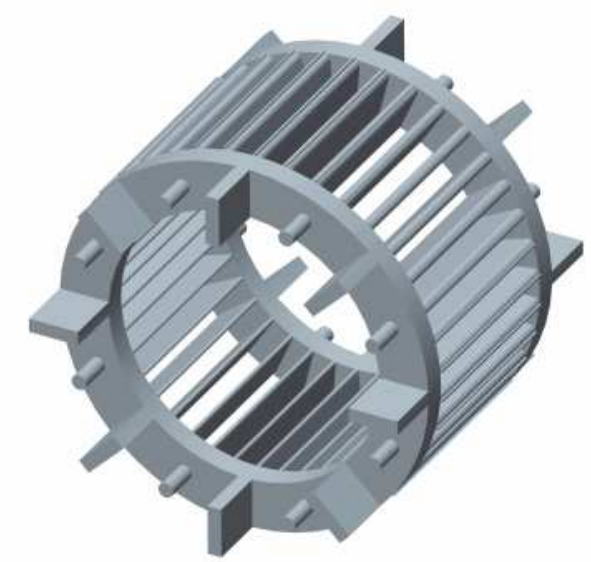

Figure 1: Rotor cage of an induction machine

In the Modelica Standard Library (MSL) the induction machines are based on the assumption, that the number of phases is limited to three and that stator and rotor windings are fully symmetrical. Electrical rotor asymmetries can therefore not be modeled using the MSL. For modeling electrical rotor asymmetries of the squirrel cage induction machines the full topology of the rotor cage has to be taken into account. Appropriate models are provided by the ExtendedMachines Library [1].

2 Stator Winding Model

For the investigated fault cases it can be assumed that the stator winding is fully symmetrical. Additionally, it will be assumed, that number of stator phases is limited to three. In this case the stator voltage equation

can be written as

$$V_{s[i]} = R_s I_{s[i]} + L_{s\sigma}\frac{\mathrm{d}I_{s[i]}}{\mathrm{d}t} + \sum_{j=1}^{3} L_{sm[i,j]}\frac{\mathrm{d}I_{s[j]}}{\mathrm{d}t} + \sum_{j=1}^{N_r}\frac{\mathrm{d}L_{sr[i,j]}I_{r[j]}}{\mathrm{d}t}. \quad (1)$$

In this equation $V_{s[i]}$ and $I_{s[i]}$ and $I_{r[i]}$ are the stator voltage and current and the rotor current, respectively. Due to the symmetry of the stator winding the stator resistance R_s and the stator stray inductance $L_{s\sigma}$ are symmetrical, too. The matrix of the main field inductances of the stator winding,

$$L_{sm[i,j]} = L_0 w_s^2 \xi_s^2 \cos\left[\frac{(i-j)2\pi}{3}\right], \quad (2)$$

and the matrix of the mutual coupling inductances between the stator and rotor,

$$L_{sr[i,j]} = L_0 w \xi_s \xi_r \cos\left[\frac{(i-1)2\pi}{3} - \frac{(j-1)2\pi}{N_r} - \gamma_m\right], \quad (3)$$

are fully symmetrical, since it is assumed that the coupling over the magnetic main field is not influenced by the rotor asymmetries. In this equation, L_0 indicates the base inductance of a coil without chording, i.e., the coil width is equal to the pole pitch. The parameters w_s and ξ_s are the number of series connected turns and the winding factor of the stator winding. The product $w_s\xi_s$ is the *effective number of turns.* The winding factor of the rotor winding

$$\xi_r = \sin\left(\frac{p\pi}{N_r}\right) \quad (4)$$

is a pure geometric factor, which is derived in [2]. In this equation, however, it is assumed that no skewing occurs [3]. The rotor angle γ_m represents the relative movement of the rotor with respect to the stator.

The effective number of turns, $w_s\xi_s$, may be determined from a winding topology, which is indicated by the begin and end location and the number of turns of the stator winding coils – as depicted in Fig. 2. Alternatively, a symmetric stator winding can be parametrized by entering the effective number of turns.

3 Rotor Winding Model

The squirrel cage rotor with N_r rotor bars can be seen as a winding topology with an effective number of turns equal to one. Using the winding factor of a rotor mesh (4), the matrix of the main rotor field can be expressed as

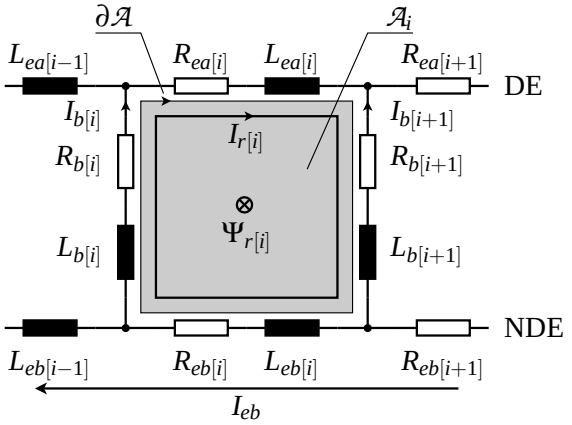

Figure 3: Topology of the rotor cage (DE = drive end, NDE = non drive end)

$$L_{rr[i,j]} = L_0 \xi_r^2 \cos\left[\frac{(i-j)2\pi}{N_r}\right]. \quad (5)$$

The rotor voltage equation can be derived from the topology of the squirrel which is depicted in Fig. 3. Considering constant leakage inductances $L_{b[i]}$ and $L_{ea[i]}$ and $L_{eb[i]}$ of the bars and the end rings on both sides (index a = drive end side, DE; index b = non drive end, NDE), the rotor voltage equations yields:

$$\begin{aligned} 0 \;=\; & (R_{ea[i]} + R_{eb[i]} + R_{b[i]} + R_{b[i+1]})I_{r[i]} \\ & - R_{b[i]}I_{r[i-1]} - R_{b[i+1]}I_{r[i]} + R_{eb[i]}I_{eb} \\ & + (L_{ea[i]} + L_{eb[i]} + L_{b[i]} + L_{b[i+1]})\frac{\mathrm{d}I_{r[i]}}{\mathrm{d}t} \\ & - \frac{\mathrm{d}}{\mathrm{d}t}(L_{b[i]}I_{r[i-1]} + L_{b[i+1]}I_{r[i]} - L_{eb[i]}I_{eb}) \\ & + \sum_{j=1}^{3}\frac{\mathrm{d}L_{sr[j,i]}I_{s[j]}}{\mathrm{d}t} + \sum L_{rr[i,j]}\frac{\mathrm{d}I_{r[j]}}{\mathrm{d}t} \end{aligned} \quad (6)$$

Additional parameters of this equation are the bar resistances $R_{b[i]}$ and the resistances of the end ring segments $R_{ea[i]}$ and $R_{eb[i]}$. The topology of the rotor cage (Fig. 4) leads to $N_r + 1$ linearly independent meshes. Therefore, the mesh current I_{eb} is introduced and the additional voltage equation

$$0 = \sum_{i=1}^{N_r} R_{eb[i]}(I_{r[i]} + I_{eb}) + \frac{\mathrm{d}}{\mathrm{d}t}\sum_{i=1}^{N_r} L_{eb[i]}(I_{r[i]} + I_{eb}) \quad (7)$$

has to be taken into account.

It should be noted that the main field inductances $L_{ss[i,j]}$ and $L_{rr[i,j]}$ of a squirrel cage induction machine

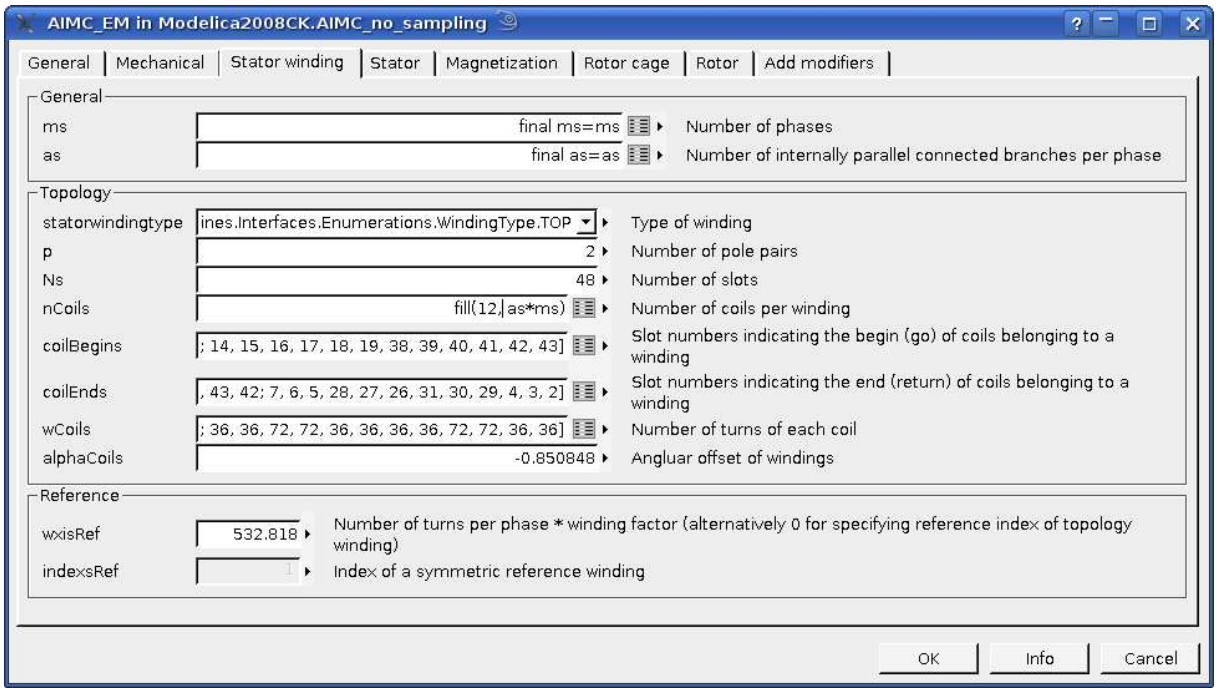

Figure 2: Stator winding parameters of a squirrel cage induction machine

are constant and the mutual inductances (3) are dependent on the rotor angle γ_m.

In the ExtendedMachines library, the rotor cage can be parametrized in two different ways. First, the resistances and leakage inductances of the rotor bars and the end ring segments of both sides can be parametrized (Fig. 4). This is how a squirrel cage is internally modeled. Second, a symmetric rotor cage can be indicated by the rotor resistance R'_r and the rotor leakage inductance $L'_{r\sigma}$, equivalently transformed to the stator side. The same parameters are used for the Machines package of the MSL. The relationship between the symmetric rotor bar and end ring resistance and the rotor resistance with respect to the stator side is determined by

$$R'_r = 2\frac{3{w_s}^2{\xi_s}^2}{N_r{\xi_r}^2}\{R_{e,\mathrm{sym}} + R_{b,\mathrm{sym}}[1-\cos(\frac{2\pi p}{N_r})]\}. \quad (8)$$

A similar equation can be obtained for the rotor leakage inductance with respect to the stator side,

$$L'_{r\sigma} = 2\frac{3{w_s}^2{\xi_s}^2}{N_r{\xi_r}^2}\{L_{e\sigma,\mathrm{sym}} + L_{b\sigma,\mathrm{sym}}[1-\cos(\frac{2\pi p}{N_r})]\}. \quad (9)$$

Additionally, the ratios of the resistances (`ratioCageR`) and leakage inductances (`ratioCageR`), each with respect to the rotor bars over the end ring segments, can be specified (Fig. 5),

$$\texttt{ratioCageR} = \frac{R_{b,\mathrm{sym}}}{R_{e,\mathrm{sym}}}, \quad (10)$$

$$\texttt{ratioCageL} = \frac{L_{b\sigma,\mathrm{sym}}}{L_{e\sigma,\mathrm{sym}}}. \quad (11)$$

This way, the symmetric cage resistance and leakage inductance parameters can be determined from R'_r, $L'_{r\sigma}$, `ratioCageR` and `ratioCageL`.

4 Torque

The electromagnetic (inner) torque of the machine is computed by

$$T_{\mathrm{el}} = \sum_{i=1}^{3}\sum_{j=1}^{N_r}\frac{\mathrm{d}L_{sr[i,j]}}{\mathrm{d}\gamma_m}I_{s[i]}I_{r[j]}. \quad (12)$$

In the presented investigation neither friction nor ventilation losses nor stray load losses are taken into account.

5 Theoretical Background of Rotor Faults

The distorted rotor bar currents have an impact on the fundamental wave of the rotor magneto motive force

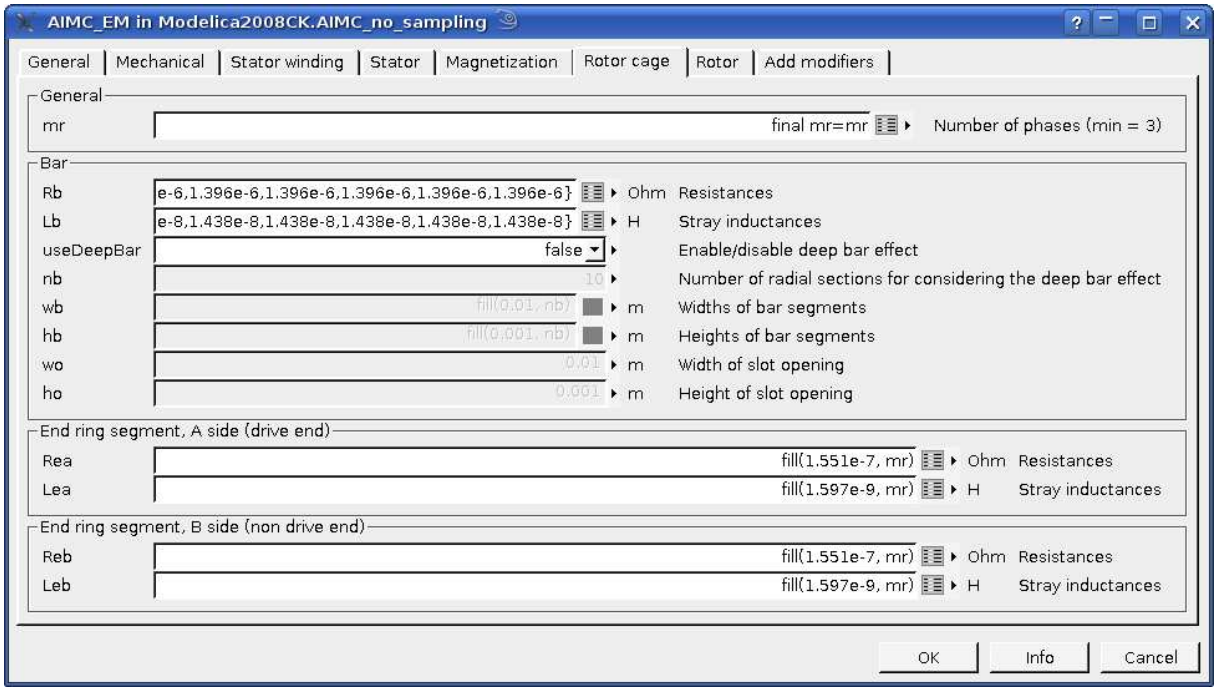

Figure 4: Parameters of the resistances and the leakage inductances of the rotor bars and end ring segments

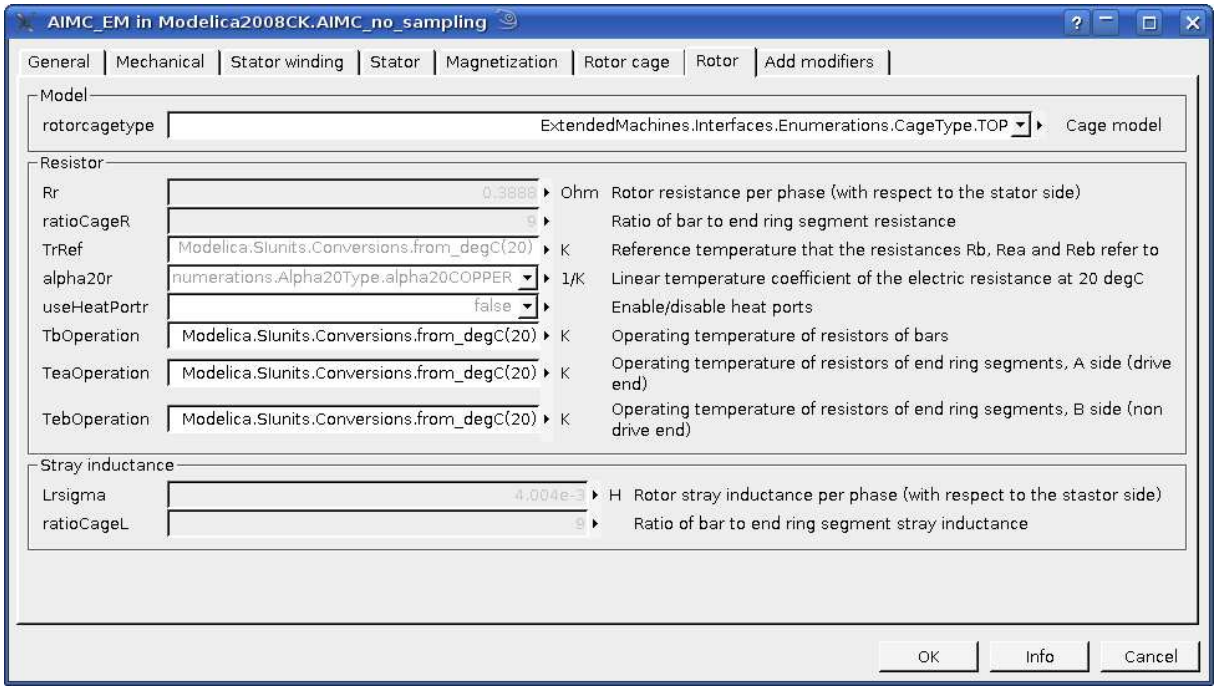

Figure 5: Parameters of the squirrel cage

Figure 6: 18.5 kW four pole induction machine

(MMF). The fundamental rotor MMF can be considered to be composed of a forward and backward traveling wave. The backward traveling wave is caused by the electrical rotor asymmetry and induces a stator voltage harmonic component at the frequency

$$f_l = (1-2s)\,f_s \tag{13}$$

for infinite inertia drives. In this equation f_s is the stator supply frequency and

$$s = \frac{f_s - pn}{f_s} \tag{14}$$

is slip, expressed in terms of rotor speed n and the number of pole pairs p. Due to the impedance of the machine (and the supply) the stator voltage harmonic gives rise to a stator current harmonic with the same frequency. To this stator current harmonic component literature refers as *lower side band* harmonic. A finite inertia of the drives gives rise to additional upper side band harmonics at the frequency

$$f_u = (1+2s)\,f_s, \tag{15}$$

the *upper side band harmonic* [4]. Between no load and rated operating conditions slip varies between zero and some per cent.

Electrical rotor asymmetries give also rise to a distortion of the magnetic field of the air gap [5] and the stray flux [6]. Additional effects are caused by the interaction of the current side band harmonics with the fundamental wave of the voltage, which gives rise to double slip frequency oscillations

$$f_t = 2s\,f_s \tag{16}$$

of the electrical power and torque [7], [8]. The magnitudes of these fault specific oscillations are much smaller the average values of the electrical power and torque, respectively.

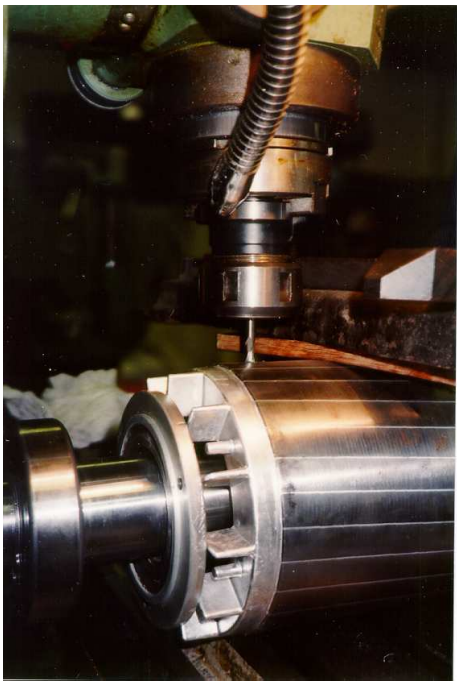

Figure 7: For broken one rotor bar a hole is drilled into the aluminum part of the squirrel cage rotor

6 Investigated Machine

Simulation and measurement results refer to a 18.5 kW, four pole induction machine with 40 rotor bars (Fig. 6). In this paper simulation and measurement results are obtained for nominal load torque, nominal line-to-line voltage (400 V) and nominal frequency (50 Hz). The investigations refer to a squirrel cage with one fully broken rotor bar. For the experiment, the faulty bar was broken by drilling a hole into the aluminum part as shown in Fig. 7.

For the investigated machine `ratioCageR=9` was estimated from the geometry, and in the same way, without getting into details, it was assumed that `ratioCageL=9`, too. With these parameters the rotor bar and end ring segment parameters $R_{b,\mathrm{sym}}$, $L_{b\sigma,\mathrm{sym}}$, $R_{e,\mathrm{sym}}$ and $L_{e\sigma,\mathrm{sym}}$ are computed according to (8)–(11) for a given rotor resistance R'_r and a leakage inductance $L'_{r\sigma}$. In the Modelica simulation the broken bar was considered by setting the faulty bar resistance with index 1

$$R_{b[1]} = 100 R_{b,\mathrm{sym}}. \tag{17}$$

This resistance increase causes the current through this bar to sufficiently vanish.

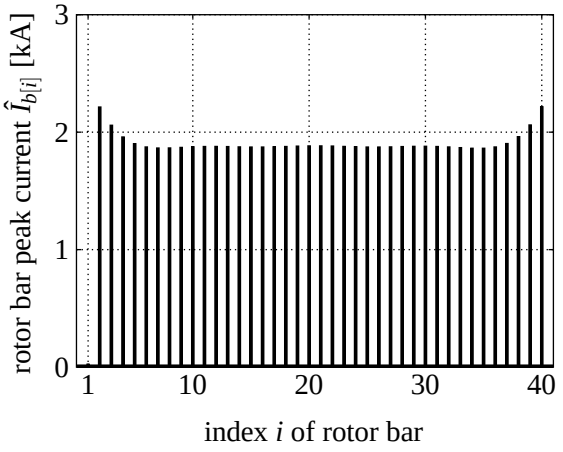

Figure 8: Peak values of the rotor bar currents; broken rotor bar with index 1; simulation results

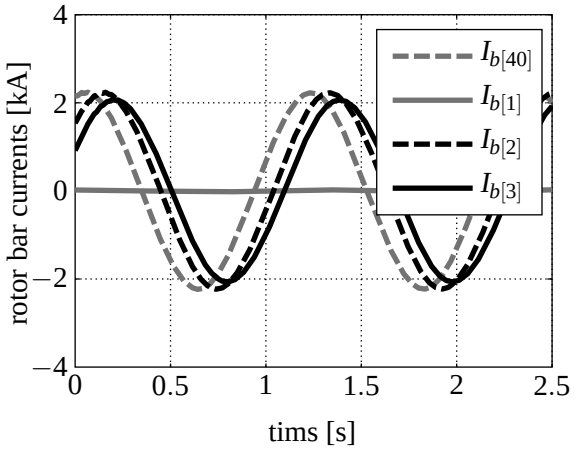

Figure 9: Rotor bar currents; broken rotor bar with index 1; simulation results

7 Simulation Results

An electrical rotor asymmetry gives rise to a distortion of the current distribution of the rotor bars and end ring segments. The rotor bar currents can be computed from the rotor currents according to Fig. 3,

$$I_{b[i]} = I_{r[i]} - I_{r[i-1]}. \tag{18}$$

For nominal load and steady state operating conditions the peak values of the the sinusoidal currents of the rotor bars are depicted in Fig. 8. A time domain plot of some these currents (index 40, 1, 2 and 3) are shown in Fig. 9. The current of the broken rotor bar (index 1) is almost zero. Additionally, an interesting phenomenon can be observed. The currents of the directly adjacent rotor bars (e.g. index 40 and 2) are significantly larger than the currents of the remaining rotor bars. Due to this effect and the associated heat losses, the thermal stress of the directly adjacent rotor bars increases. This may also cause a damage of the adjacent bars which gives rise to an avalanche-like increase of the extend of the damage. Nevertheless, electrical rotor asymmetries spread relatively slow compared to other machine faults. A significant rise of the fault extend may thus happen within weeks, months or even years.
Due to the distortion of the current distribution in the rotor bars, the end ring current distribution changes, too. The rotor end ring currents of the A- and B-side can be defined by

$$I_{ea[i]} = I_{r[i]}, \tag{19}$$
$$I_{eb[i]} = I_{r[i]} + I_{eb}. \tag{20}$$

Without any asymmetry of either of the end rings, $I_{eb} = 0$ applies and therefore the currents of the A- and B-side are equal. The peak values of the currents of the rotor end ring segments are depicted in Fig. 10.

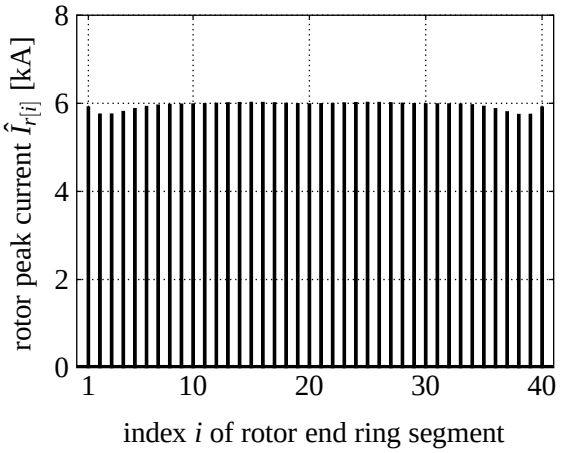

Figure 10: Peak values of the currents of the end ring segments; broken rotor bar with index 1; simulation results

The lower and upper side band harmonics of the current arise a few Hertz differing from the fundamental wave according to (13) and (15). For the investigated machine 50 Hz machine the Fourier spectrum of a stator current (phase 1) is depicted in Fig. 11. The lower and upper side band harmonics clearly arise at 48.6 Hz and 51.4 Hz. The magnitudes of these side band components are, however, much smaller than the magnitude of the fundamental. Therefore, electrical rotor asymmetries can usually not be determined from the time domain waveforms.

8 Measurement Results

The measured Fourier spectrum of on stator phase current is depicted in Fig. 12. Comparing this plot with

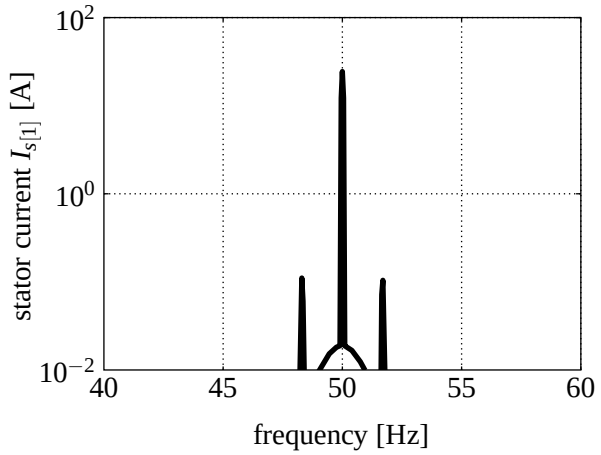

Figure 11: Fourier spectrum of the stator current $I_{s[1]}$; simulation results

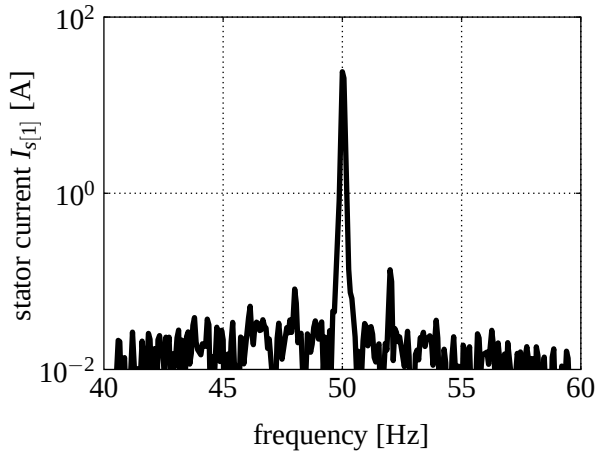

Figure 12: Fourier spectrum of the stator current $I_{s[1]}$; measurement results

the simulation results of Fig. 11 reveals, that the frequencies of the side band harmonics are the same, but the magnitudes show small deviations. The different magnitude of the side band harmonics is mainly related with the inertia of the drive which is not perfectly tuned such way that the magnitudes match. Additionally, due to the deviation of the modeled rotor bar and end ring resistance ratio from the real machine cage, some deviations in the simulation results may arise. With respect to the comparison of measurement and simulation results it should also be noted that in a real motor interbar currents can arise [9], which are not modeled in the ExtendedMachines library. These interbar currents lead to a current flow through the rotor teeth, first, in general, and, second, adjacent to the broken bar. Therefore, interbar currents may have an impact on the magnitudes of the side band currents.

9 Rotor Fault Detection Methods

Only severe rotor asymmetries can be detected through significant fluctuations of the amperemeters or wattmeters connected in the feeders of the machine. Upcoming electric rotor asymmetries require some more sophisticated detection methods. The most usual rotor fault detection methods are solely based on the measurement of one stator current. This class of methods is called *current signature analysis* (CSA) methods [10], [11], [12]. The measured current is then processed by either a fast Fourier transform [13] or a wavelet transform [14], [15] or some other signal processing techniques.

A second class of methods is based on *power signature analysis* (PSA), evaluating either total or phase power [7]. Additionally to CSA or PSA techniques, neural networks [16], [17] or Fuzzy based methods [18] may be applied.

A third class uses model based techniques for detecting a rotor fault. One model based technique is the Vienna Monitoring Method (VMM) which was introduced in 1997 [19]. This method evaluates two mathematical machine models and calculates torque for each model. In case of a fully symmetrical machine both models calculate the same torque and torque difference is zero. An electrical rotor asymmetry gives rise to side band currents and double slip frequency torque oscillations. These torque oscillations are differently sensed by the two mathematical models due to the different model structure. This leads to different magnitudes and phase shifts of the double slip frequency torque oscillation derived by the two models. Therefore, torque difference shows a double slip frequency oscillation which indicates an electrical rotor fault.

The torque difference, divided by the average load torque, serves as quantity to determine the fault indicator through a certain data clustering technique. The fault indicator is basically the magnitude of the double slip frequency oscillation of the torque difference, divided by the average load torque. The particular advantage of the VMM is that it provides a reliable fault indicator independent of load torque, speed, supply and inertia of the drive [20], [21], [22].

The VMM has been applied to both the simulation and measurement results. For the simulation results the determined fault indicator is 0.0093 and the VMM applied to the measured data leads to a fault indicator of 0.0105. This is a deviation of about 11%. Considering no parameter tuning of the simulation model this is a satisfactory result.

10 Conclusions

For squirrel cage induction machines the background of electrical rotor asymmetries is discussed. A rotor topology models for handling cage asymmetries is introduced and the implementation in the ExtendedMachines library is presented.
A 18.5 kW induction machine with one broken rotor bar out of 40 bars is investigated. The simulated and measured stator current Fourier spectrum are compared and shown good coherence. Additionally, the simulation and measurement data are applied to a model based rotor fault detection method – the Vienna Monitoring Method. The comparison of the two fault indicators determined by the Vienna Monitoring Method reveals a deviation of about 11%. Considering that no parameter tuning of the simulation model has been performed, this is a satisfactory matching result.

References

[1] C. Kral, A. Haumer, and F. Pirker, "A modelica library for the simulation of electrical assymetries in multiphase machines - the extended machines library," *IEEE International Symposium on Diagnostics for Electric Machines, Power Electronics and Drives, The 6th, SDEMPED 2007, Cracow, Poland*, 2007.

[2] C. Kral, *Modellbildung und Betriebsverhalten einer Asynchronmaschine mit defektem Rotorstab im Läuferkäfig einschließlich Detektion durch die Vienna Monitoring Method*. PhD thesis, Technische Universität Wien, 1999.

[3] G. Müller, *Elektrische Maschinen - Theorie rotierender elektrischer Maschinen*. Berlin: VEB Verlag Technik, 2 ed., 1967.

[4] F. Filippetti, G. Franceschini, C. Tassoni, and P. Vas, "Impact of speed riple on rotor fault diagnosis of induction machines," *Proceedings of the International Conference on Electrical Machines, ICEM*, pp. 452–457, 1996.

[5] M. Schagginger, *Diplomarbeit-Luftspaltfelduntersuchungen an umrichtergespeisten Asynchronmaschinen im Hinblick auf elektrische Unsymmetrien im Rotorkäfig*. Wien: TU, 1997.

[6] H. Henao, C. Demian, and G.-A. Capolino, "A frequency-domain detection of stator winding faults in induction machines using an external flux sensor," *Issue: 5 Industry Applications, IEEE Transactions on , Volume: 39*, pp. 1272–1279, 2003.

[7] Z. Liu, X. Yin, Z. Zhang, D. Chen, and W. Chen, "Online rotor mixed fault diagnosis way based on spectrum analysis of instantaneous power in squirrel cage induction motors," *IEEE Transactions on Energy Conversion*, vol. 19, pp. 485–490, Sept. 2004.

[8] S. Legowski, A. S. Ula, and A. Trzynadlowski, "Instantaneous power as a medium for the signature analysis of induction motors," *IEEE Transactions on Industry Applications*, vol. 32, no. 4, pp. 904–909, 1996.

[9] R. Walliser, "The influence of interbar currents on the detection of broken rotor bars," *ICEM*, pp. 1246–1250, 1992.

[10] M. Benbouzid, "A review of induction motors signature analysis as a medium for fault detection," *Annual Conference of the IEEE Industrial Electronics Society, IECON*, pp. 1950–1955, 1998.

[11] A. Bellini, F. Filippetti, G. Franceschini, C. Tassoni, R. Passaglia, M. Saottini, G. Tontini, M. Giovannini, and A. Rossi, "On-field experience with online diagnosis of large induction motors cage failures using mcsa," *IEEE Transactions on. Industry Applications*, vol. 38, no. 4, pp. 1045–1053, 2002.

[12] G. Didier, E. Ternisien, O. Caspary, and H. Razik, "Fault detection of broken rotor bars in induction motor using a global fault index," *IEEE Transactions on Industry Applications*, vol. 42, pp. 79–88, Jan.-Feb. 2006.

[13] I. M. Culbert and W. Rhodes, "Using current signature analysis technology to reliably detect cage winding defects in squirrel-cage induction motors," *IEEE Transactions on Industry Applications*, vol. 43, pp. 422–428, March-april 2007.

[14] H. Douglas, P. Pillay, and A. Ziarani, "Broken rotor bar detection in induction machines with transient operating speeds," *IEEE Transactions on Energy Conversion*, vol. 20, pp. 135–141, Mar 2005.

[15] J. Antonino-Daviu, M. Riera-Guasp, J. Folch, and M. Palomares, "Validation of a new method for the diagnosis of rotor bar failures via wavelet transform in industrial induction machines," *IEEE Transactions on Industry Applications*, vol. 42, pp. 990–996, July-August 2006.

[16] B. Ayhan, M.-Y. Chow, and M.-H. Song, "Multiple discriminant analysis and neural-network-based monolith and partition fault-detection schemes for broken rotor bar in induction motors," *IEEE Transactions on Industrial Electronics*, vol. 53, pp. 1298–1308, June 2006.

[17] W. W. Tan and H. Huo, "A generic neurofuzzy model-based approach for detecting faults in induction motors," *IEEE Transactions on Industrial Electronics*, vol. 52, pp. 1420–1427, Oct. 2005.

[18] E. Ritchie, X. Deng, and T. Jokinen, "Diagnosis of rotor faults in squirrel cage induction motors using a fuzzy logic approach," *Proceedings of the International Conference on Electrical Machines, ICEM*, pp. 348–352, 1994.

[19] R. Wieser, C. Kral, F. Pirker, and M. Schagginger, "On-line rotor cage monitoring of inverter fed induction machines, experimental results," *Conference Proceedings of the First International IEEE Symposium on Diagnostics of Electrical Machines, Power Electronics and Drives, SDEMPED*, pp. 15–22, 1997.

[20] C. Kral, F. Pirker, and G. Pascoli, "Influence of load torque on rotor asymmetry effects in squirrel cage induction machines including detection by means of the Vienna Monitoring Method," *Conference Proceedings EPE*, 2001.

[21] C. Kral, H. Kapeller, J. Gragger, F. Pirker, and G. Pascoli, "Detection of mechanical imbalances during transient torque operating conditions," *5th IEEE International Symposium on Diagnostics for Electric Machines, Power Electronics and Drives, SDEMPED*, 2005.

[22] C. Kral, F. Pirker, and G. Pascoli, "The impact of inertia on rotor faults effects - theoretical aspects of the Vienna Monitoring Method," *IEEE International Symposium on Diagnostics for Electric Machines, Power Electronics and Drives, The 6th, SDEMPED 2007, Cracow, Poland*, 2007.